



Experimental analysis of manufacturing parameters' effect on the flexural properties of wood-PLA composite parts built through FFF

M. Damous Zandi¹ · Ramon Jerez-Mesa² · Jordi Lluma-Fuentes³ · Joan J. Roa³ · J. Antonio Travieso-Rodriguez¹

Received: 4 November 2019 / Accepted: 27 December 2019 / Published online: 10 January 2020
© Springer-Verlag London Ltd., part of Springer Nature 2019

Abstract

This paper aims to determine the flexural stiffness and strength of a composite made of a polylactic acid reinforced with wood particles, named commercially as Timberfill, manufactured through fused filament fabrication (FFF). The influence of four factors (layer height, nozzle diameter, fill density, and printing velocity) is studied through an L_{27} Taguchi orthogonal array. The response variables used as output results for an analysis of variance are obtained from a set of four-point bending tests. Results show that the layer height is the most influential parameter on flexural strength, followed by nozzle diameter and infill density, whereas the printing velocity has no significant influence. Ultimately, an optimal parameter set that maximizes the material's flexural strength is found by combining a 0.2-mm layer height, 0.7-mm nozzle diameter, 75% fill density, and 35-mm/s velocity. The highest flexural resistance achieved experimentally is 47.26 MPa. The statistical results are supported with microscopic photographs of fracture sections, and validated by comparing them with previous studies performed on non-reinforced PLA material, proving that the introduction of wood fibers in PLA matrix reduces the resistance of raw PLA by hindering the cohesion between filaments and generating voids inside it. Lastly, five solid Timberfill specimens manufactured by injection molding were also tested to compare their strength with the additive manufactured samples. Results prove that treating the wood-PLA through additive manufacturing results in an improvement of its resistance and elastic properties, being the Young's module almost 25% lower than the injected material.

Keywords Additive manufacturing · 3D printing · Fused filament fabrication · Young's module · Flexural strength · Timberfill

Abbreviations

AM	Additive manufacturing
FFF	Fused filament fabrication
DOE	Design of experiments
ANOVA	Analysis of variance

1 Introduction

Among all the additive manufacturing (AM) technologies, the most popular is fused deposition modeling (FDM), also referred to as fused filament fabrication (FFF) [1]. This is due to its economic accessibility, ease of use, and variety of materials commercially available [2]. These kinds of technologies offer the potential for significant cost savings due to reduced material waste and the production of intricate geometries. Therefore, they have gained considerable attention during the last decades. An FFF printer generates a 3-dimensional object by extruding a stream of heated and semi-melted thermoplastic material, which is deposited onto layer upon layer, working from the bottom up. This process is performed by means of a heated print head that is oozing out a permanent flow of that semi-molten plastic. The deposited material will almost immediately harden upon leaving the hot print head, thus materializing in a small period of time the desired workpiece [3].

✉ Ramon Jerez-Mesa
ramon.jerez@uvic.cat

¹ Escola d'Enginyeria de Barcelona Est, Mechanical Engineering Department, Universitat Politècnica de Catalunya, Av. Eduard Maristany, 10-14, 08019 Barcelona, Spain

² Faculty of Sciences and Technology, Engineering Department, Universitat de Vic-Universitat Central de Catalunya, C. Laura 13, 08500 Vic, Spain

³ Escola d'Enginyeria de Barcelona Est, Materials Science and Metallurgical Engineering Department, Universitat Politècnica de Catalunya, Av. Eduard Maristany, 10-14, 08019 Barcelona, Spain

The increase in accessibility of FFF machines has inspired the scientific community to work towards the understanding of the structural performance of components fabricated with this technology. During the last years, numerous researches have focused on studying the influence of the building parameters on different mechanical properties. The existence of a high variety of parameters that influence the results of additive manufacturing makes it difficult to choose the best combination suitable to optimize the mechanical characteristics of the part for final use. Usually, operators choose these parameters under their experience and acquired knowledge, but there is not enough comprehensive information to determine them from a scientific point of view, or at least confirmed by experimental evidence [4]. Afrose et al. [5] developed an experimental analysis of fatigue characteristics by considering the effect of different build orientations. It was observed that the ultimate tensile stress of polylactic acid (PLA) samples built in the x direction was the highest at 38.7 MPa and ranged from 60 to 64% of the raw PLA material. Gomez-Gras et al. [6] studied the influence of the infill density and pattern, nozzle diameter, layer height, and printing speed on fatigue performance of cylindrical specimens, and found a lower threshold for the fatigue endurance limit at 35.8 MPa. In that research, the honeycomb infill pattern was also advised to manufacture FFF parts, as it enabled a longer lifespan with regard to specimens manufactured using a rectilinear infill. Further studies by Es Said et al. [7] show that the raster orientation defines the alignment direction of the polymer molecules, making the additive manufactured parts highly anisotropic. Wu et al. [8] devoted a study to evaluate the influence of the layer thickness and the raster angle on the mechanical properties of polyetherether-ketone (PEEK) pieces. Samples with three different layer thicknesses (200, 300, and 400 μm) and raster angles (0° , 30° , and 45°) were built, and their tensile, compressive, and bending strengths were tested. The optimal mechanical properties of the samples were found at a layer thickness of 300 μm and a raster angle of 0° . Furthermore, a comparison with acrylonitrile butadiene styrene (ABS) parts proved that the average tensile strengths of PEEK parts higher than those for ABS, indicating its interest from an industrial point of view in substituting the use of ABS.

Authors have also typically applied techniques other than statistical analysis of mechanical tests. For instance, Shabat et al. [9] performed the mechanical and structural characterization of FDM of ABS modeling material by visual testing and light microscopy. The test results revealed different fracture surfaces depending to the different building strategies. The fracture modes revealed greater ductility for specimens built horizontally. Similar results were reached by Kumar Sood et al. [10], considering the influence of five important process parameters such as layer thickness, orientation, raster angle, raster width, and air gap on three responses (tensile, flexural, and impact strength) of test specimen.

On the other hand, Araya-Calvo et al. [11] conducted mechanical characterization of AM technology based on composite filament fabrication (CFF), which utilizes a similar method of layer by layer printing as FFF through experimental design, to investigate the effect of fiber pattern, reinforcement distribution, and print orientation on compressive and flexural mechanical properties of polyamide 6 (PA6) reinforced with continuous carbon fiber (CF). In this work, maximized flexural response is achieved with 0.4893 carbon fiber volume ratio, concentric reinforcement and perpendicular to the applied force, resulting in a flexural modulus of 14.17 GPa and a proportional limit of 231.1 MPa. Another study focused on the influence of nozzle temperature and infill line orientations for parts made with short CF-reinforced PLA. Results have shown the influence of nozzle temperature on the mechanical properties, with an optimum temperature maximizing the tensile properties. Infill orientations also play a significant role in achieving good mechanical properties, with the proper combination of orientation enabling the tailoring of properties along a specific axis [12].

To reduce the consumption of petroleum-based resources and thereby enhance the eco-friendliness of the material, it could be interesting to replace of parts of ABS with other materials such as PLA or other composites and renewable materials for same purposes. To this extent, other researches have compared the mechanical characterizations of different materials [13–15]. Tymrak et al. [16] quantified the basic tensile strength/stress and elastic modulus of printed ABS and PLA components using realistic environmental conditions for standard users of a selection of low-cost, open-source 3-D printers. The results show that the average tensile strength of RepRap printed parts is 28.5 MPa for ABS and 56.6 MPa for PLA with average elastic module of 1807 MPa for ABS and 3368 MPa for PLA. These results indicate that the 3-D printed components from RepRaps are comparable in tensile strength and elastic modulus to the parts printed on commercial 3-D printing systems. While considerations must be made for the settings, tuning, and operation of each individual printer as well as the type, age, and quality of polymer filament used, functionally strong parts can be created with open-source 3-D printers within the bounds of their mechanical properties. Ali Bagheri et al. [17] analyzed the mechanical behavior of octet-truss microstructures of scaffold stiffness made of PLA. Through this study, the effect of the struts radius on the structure stiffness was assessed. The results have shown that higher density delivers higher values of the module elasticity.

Also several researchers considered different mechanical behaviors of parts fabricated through another different manufacturing technologies [18–20], and different treatments on the raw materials and building conditions [21–24]. Amin Abedini et al. [25] studied the effects of the percentage of Al_2O_3 nanoparticles in an ABS matrix and injection molding

process parameters on the mechanical and thermal properties of nanocomposites. Tensile and impact tests evidenced that Al_2O_3 nanoparticles decreased the impact strength of the nanocomposites. On the other hand, the effects of injection molding process parameters were statistically insignificant which imply more flexibility on selecting the injection molding processing conditions. Another study [26] investigated deep drawing process of brass-steel laminated sheets from the required forming load and thickness reductions points of view. It was observed that the friction coefficient of steel was the most important parameter influencing thickness reductions of both sheets with 41 and 39% contributions, respectively. To achieve higher resistances of mechanical properties, many contradictions still need to be considered, including the high costs associated with these commercial machines, their material restrictions, and the difficulty to study process parameters [27].

As observed in the presented state of the art, the exploration of mechanical properties of workpieces generated through additive manufacturing has been extensively tackled with. However, references only focus on the typical PLA and ABS materials, neglecting the existence of other raw materials that can be manufactured through FFF. For this reason, the aim of this work is to characterize an innovative PLA-wood composite by studying the influence of printing parameters on the one provided by Filamentum Ltd. under the commercial name of Timberfill. Results shall be extracted from a four-point bending tests to determine an optimal set of parameters to improve flexural strength. Taguchi L_{27} orthogonal array design is used in the experimental phase to avoid manufacturing a large amount of runs. Then, to evaluate the achieved characteristics of flexural property of printed Timberfill samples, a comparison was made between the mechanical properties of printed PLA and injected Timberfill parts using the same test procedure.

2 Materials and methods

2.1 Four-point bending testing and specimens

The specimens are manufactured with 2.85 mm of diameter Timberfill Champagne, developed and manufactured by Filamentum Ltd. To achieve that objective, the company developed a composition of biodegradable PLA polymer combined with wood fibers in a 10% ratio. This material is provided as a commodity, with the purposes of becoming a commonly used material in FFF machines for various applications, hence the interest of characterizing and understanding its performance when treated through a FFF process. Table 1 includes the technical information provided by the manufacturer.

Table 1 Initial mechanical properties and manufacturer recommendations of printing parameters of Timberfill material

Property	Value	Property	Value
Material density	1.26 g/cm ³	Nozzle temperature	170–185 °C
Tensile strength ^a	39 MPa	Nozzle diameter	Min. 0.4 mm
Tensile modulus ^a	3200 MPa	Extruder velocity	20–30 mm/s

^aMinimum guaranteed by the manufacturer

The four-point flexural test was performed on prismatic specimens with dimensions according to the ASTM D6272 standard [28]. This testing method details the procedure to determine the flexural properties of unreinforced and reinforced plastics, including high-modulus composites and electrical insulating materials in different forms. Hence its adequacy for the purposes of these works with a composite material.

The test consists on a bar of rectangular cross-section resting on two supports, which is loaded at two points by means of the respective loading noses, each one with an equal distance from the adjacent support point. The distance between the noses (the load span) is either one third or one half of the support span. A support span-to-depth ratio of 16:1 shall be used. The loading noses and supports shall have cylindrical surfaces. In order to avoid excessive indentation or failure due to stress concentration directly under the loading noses, the radii of the loading noses and supports should be 5 ± 0.1 mm. According to this method, the distances between support spans and load spans shall be 64 and 21.3 mm, respectively.

The machine is adjusted as near as possible to that calculated rate for the load span of one third of the support span. Once the conditions are determined, displacement rate of 19 mm/min and maximum displacement of 10.98 mm are achieved.

2.2 Taguchi experimental design

The Design of Experiments (DOE) technique has been used to carry out the study. In this work, four parameters varying in three levels are included in the model. Table 2 shows the factors and their selected levels to be developed based on a Taguchi experimental design method which is a robust optimization technique to make experimental to predict responses

Table 2 Factors and levels used for the DOE

Parameter	Levels		
	1	2	3
Layer height (mm)	0.2	0.3	0.4
Nozzle diameter (mm)	0.5	0.6	0.7
Infill density (%)	25	50	75
Printing velocity (mm/s)	25	30	35

and optimize the FFF process conditions in accuracy level [29]. These factors and levels were selected based on a preliminary set of tests out of the experimental design of this paper, to confirm and adjust the recommendations given by the material manufacturer. Since the layer height should be almost half of the nozzle diameter, the selected layer height values are based on the nozzle diameter.

To analyze the influence of these factors, a L_{27} Taguchi orthogonal array was used to conduct the experimental phase (Table 3). Of each manufacturing parameter set or run included in the array, 5 specimens were manufactured and tested, to guarantee the repeatability of the results. Once the results were obtained, the statistical calculations were performed by the Minitab 18 software, and the interactions between the different parameters were analyzed which leads to the conclusion if there is significant interaction among the pairs of selected values or not, since the p values of each pairs should be less than 0.05.

It should be taken into account that all of the samples are printed with honeycomb infill pattern. Therefore, the rest of the parameters that are not object of study have been kept constant

among all specimens (orientation 0-X, raster angle 45°, nozzle temperature 180 °C, infill pattern honeycomb, and 2 skirt layers).

2.3 Specimens manufacture

According to the ASTM testing method, the specimens may be cut from sheets, plates, or molded shapes, or may be molded to the desired finished dimensions. Their actual dimensions and shape are a parallelepiped with $10 \times 8 \times 4$ mm.

2.4 Experimental setup

The four-point bending experiments were conducted using a ZwickRoell Z020, electromechanical multi-space machine with a maximum load of 20 kN. A 500-N load cell was connected to a Spider 8 data acquisition system to record the force applied every sampling instant during the test and transfer the data to the computer. On the other hand, the specimen was recorded through an HD camera at 60-Hz sampling frequency. The camera was also equipped with a switch-controlled flash to illuminate the test area and to synchronize the data. Like

Table 3 L_{27} Taguchi orthogonal array of DOE

Run	Layer height (mm)	Nozzle diameter (mm)	Infill density (%)	Printing velocity (mm/s)
1	0.2	0.5	25	25
2	0.2	0.5	50	30
3	0.2	0.5	75	35
4	0.2	0.6	25	35
5	0.2	0.6	50	30
6	0.2	0.6	75	25
7	0.2	0.7	25	35
8	0.2	0.7	50	25
9	0.2	0.7	75	30
10	0.3	0.5	25	30
11	0.3	0.5	50	35
12	0.3	0.5	75	25
13	0.3	0.6	25	35
14	0.3	0.6	50	25
15	0.3	0.6	75	30
16	0.3	0.7	25	25
17	0.3	0.7	50	30
18	0.3	0.7	75	35
19	0.4	0.5	25	35
20	0.4	0.5	50	25
21	0.4	0.5	75	30
22	0.4	0.6	25	25
23	0.4	0.6	50	30
24	0.4	0.6	75	35
25	0.4	0.7	25	30
26	0.4	0.7	50	35
27	0.4	0.7	75	25

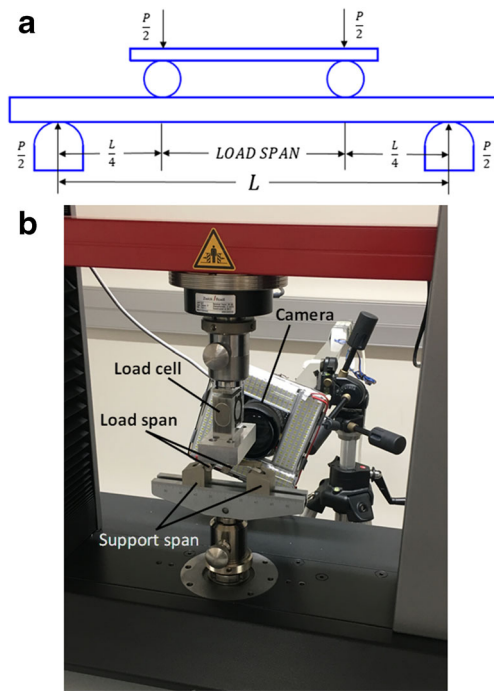


Fig. 1 a. Geometry and loading system of the four-point bending test. b Universal testing machine ZwickRoell Z020 used to conduct the tests with camera and load equipment assembly

that, strain was computed as a result of a Matlab routine based on image processing functions through which the frames were translated into displacement. Figure 1 shows the standard loading system and test equipment assembly.

2.5 Analyzing process

The described equipment was applied to carry out the tests on all of the 135 FFF samples. Furthermore, five additional specimens were manufactured with the same raw material through

injection, to compare the results of additive manufactured parts with a reference value. After each test was completed, two different files were generated. Firstly, a file that contains the force collected from the load cell, as well as the recorded voltage versus time. Secondly, the video recorded by the camera that provided graphical information to compute the strain of the specimen at every stage of the test.

The constructed stress-strain figure for every specimen was used to extract different mechanical descriptors used as response variables for the ANOVA model. These were the Young's modulus (E), the elastic limit ($S_{0.2}$), the maximum stress or flexural strength (σ_{\max}), and maximum deformation (e_{\max}). A self-designed Matlab routine was executed in a Matlab R2018b software. Essentially, the routine performs the following steps:

- The input data is the HD video processed during the test, and it is firstly divided into its different frames. Since the camera captures 60 frames per second, and the average duration of the test is 50 s, the average number of frames to process for each test is 3000.
- The video frames and the recorded force data are synchronize. When the test starts, the flash is activated and sends a 0-V signal to the DAQ Spider system to launch data recording. Subsequently, the Matlab script synchronizes the dark frame of the video and the Spider data recorded alongside at the same time. Then, it detects the points until the maximum bending position before the sample will be broken.
- A grid is generated in the initial frame of the test sample. This gridding consists of a straight line divided by 50 points at the outer fiber and two rectangular grids at the support spans (Fig. 2a). It is important that the linear grid extends the space between both loading points.
- Deflection is computed by tracking every marked pixels, based on the differences between the initial and final

Fig. 2 a Generated grid with Matlab ® script. b Image processing protocol. c Calculation of the pixel/millimeter ratio

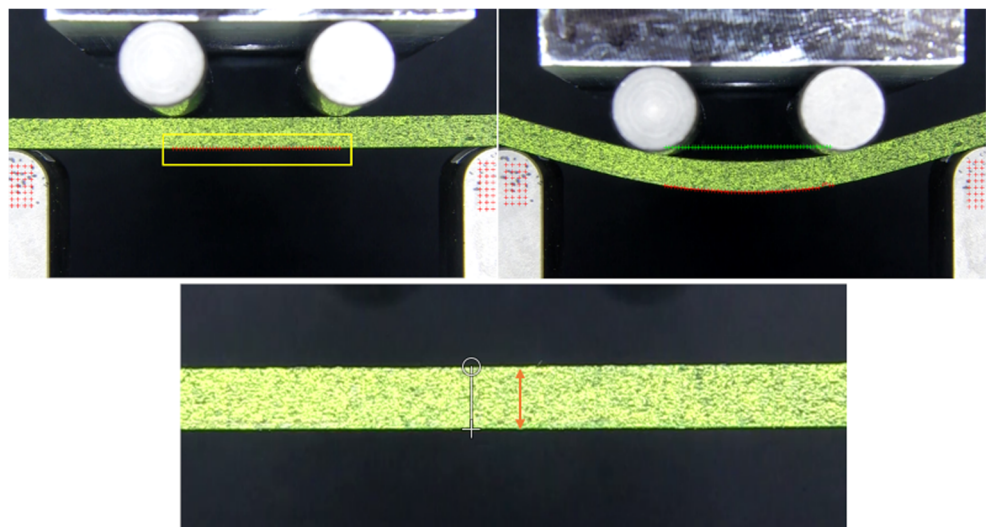
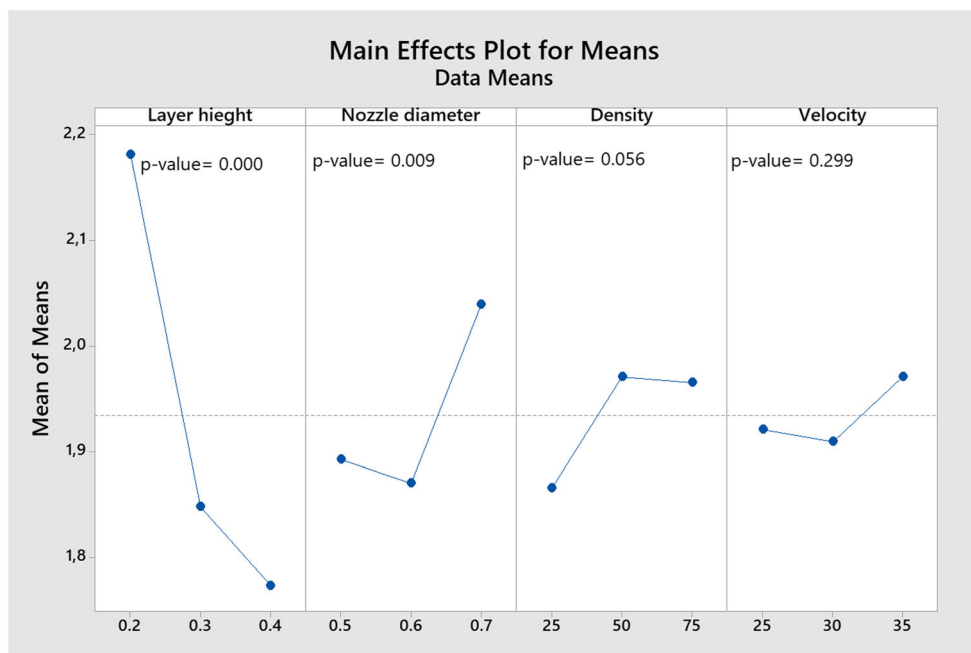


Table 4 Results obtained for each experimental run including standard deviations

	<i>E</i> (GPa)	<i>S</i> _{0,2} (MPa)	δ_{max} (MPa)	<i>e</i> _{max} (%)
1	2.07 ± 0.08	30.66 ± 0.56	35.34 ± 0.34	2.77 ± 0.34
2	2.13 ± 0.04	33.48 ± 0.77	39.52 ± 1.25	3.49 ± 0.33
3	2.17 ± 0.04	34.19 ± 0.42	41.15 ± 0.88	4.65 ± 1.78
4	2.03 ± 0.08	31.56 ± 0.91	37.82 ± 0.49	3.46 ± 0.08
5	2.12 ± 0.04	31.83 ± 0.97	39.76 ± 0.93	4.35 ± 0.00
6	2.16 ± 0.05	32.96 ± 0.47	40.45 ± 0.64	3.92 ± 0.45
7	2.29 ± 0.15	36.28 ± 0.56	44.17 ± 1.82	4.07 ± 0.68
8	2.24 ± 0.08	35.73 ± 0.56	45.40 ± 0.99	5.34 ± 1.62
9	2.41 ± 0.04	38.06 ± 1.71	47.26 ± 0.86	4.24 ± 0.31
10	1.76 ± 0.07	28.45 ± 1.05	34.29 ± 0.68	3.80 ± 0.32
11	1.89 ± 0.05	29.54 ± 0.81	36.26 ± 0.58	4.70 ± 1.68
12	1.77 ± 0.06	29.56 ± 0.71	36.24 ± 0.64	4.72 ± 1.99
13	1.82 ± 0.07	36.58 ± 1.62	34.94 ± 1.37	3.80 ± 0.73
14	1.87 ± 0.08	29.69 ± 0.52	37.46 ± 0.66	4.07 ± 0.14
15	1.82 ± 0.06	28.97 ± 1.05	35.51 ± 2.40	3.96 ± 0.61
16	1.84 ± 0.07	29.27 ± 1.24	36.64 ± 1.29	4.48 ± 0.44
17	1.91 ± 0.08	29.49 ± 1.07	37.01 ± 1.83	3.86 ± 0.44
18	1.94 ± 0.08	30.40 ± 1.62	40.17 ± 1.67	4.89 ± 0.37
19	1.70 ± 0.09	26.60 ± 1.78	26.04 ± 2.03	3.15 ± 1.76
20	1.81 ± 0.08	27.53 ± 0.31	33.19 ± 0.70	3.62 ± 0.31
21	1.73 ± 0.11	27.74 ± 0.64	35.14 ± 1.43	4.57 ± 0.62
22	1.41 ± 0.08	23.32 ± 1.78	27.05 ± 2.25	3.59 ± 0.76
23	1.69 ± 0.11	27.23 ± 0.94	32.97 ± 2.14	4.04 ± 0.50
24	1.89 ± 0.20	29.43 ± 5.46	35.64 ± 7.74	3.88 ± 0.90
25	1.86 ± 0.03	30.71 ± 0.53	37.99 ± 0.81	4.64 ± 0.24
26	1.91 ± 0.09	31.35 ± 1.21	39.79 ± 1.52	4.79 ± 0.26
27	1.95 ± 0.15	31.09 ± 1.61	40.27 ± 1.23	4.80 ± 0.53

position. The results are converted into an array at the X-axis and Y-axis separately. The difference between the positions in the current frame (in red) and the starting position (in green) is shown in Fig. 2 b. By finishing this step, two scroll

Fig. 3 Main effect for means calculated through ANOVA. Response variable: Young’s module



- files were generated and introduced into a specific script to compute the real deformation of the specimens’ outer fibers.
- All deformations for every frame is calculated as described in the previous point, and the whole flexural curve is created. The pixels that have been measured by Matlab are converted in millimeters. The GIMP 2.10.8 software is used to do this, as can be seen in Fig. 2 c.
- By means of another Matlab script, the voltage and the deformation are calculated for the specimen second by second, and the results are synchronized with the deformations value that have been calculated previously. Finally a .txt format file is generated with voltage, deformation versus time. Consequently, the stress is calculated by the Euler-Bernoulli equation for a rectangular section beam subjected to pure bending stress (Eq. 1)

$$S = \frac{PL}{bd^2} \tag{1}$$

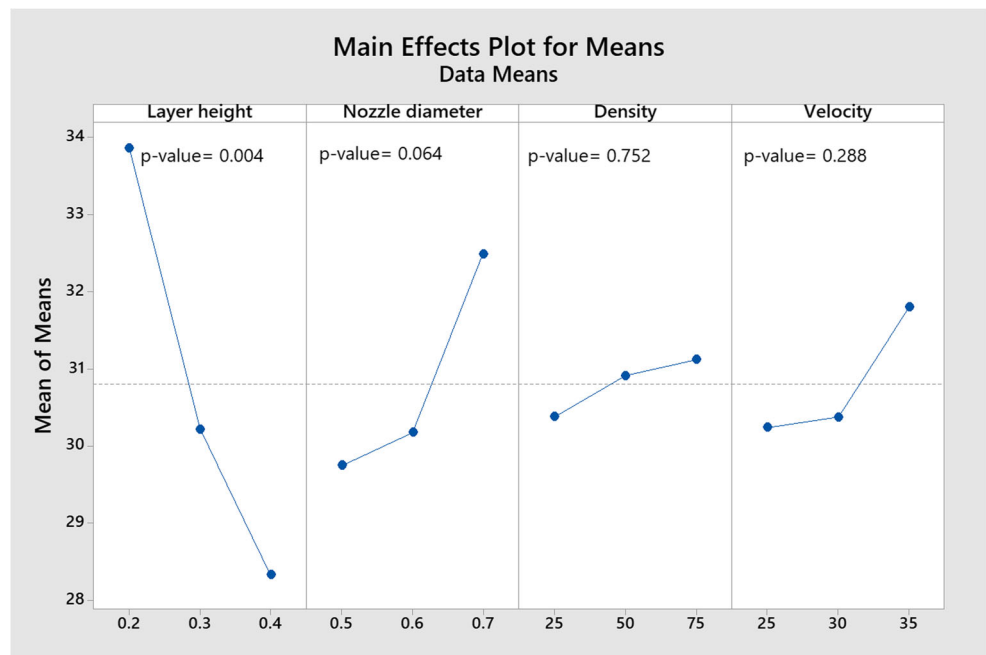
where *S* is the stress applied to the external fiber, *P* is the load, *L* is the specimen length, *b* is the specimen width, and *d* is the specimen thickness.

Here the average value of thickness and width is defined by measuring manually the specimen before the test with a micrometer.

2.6 Comparison between Timberfill and PLA

Since Timberfill is a composite of PLA and wood fibers, it is interesting to compare the results achieved on Timberfill material with its base material, as it is an extended material and is

Fig. 4 Main effect for mean effects calculated through ANOVA. Response variable: elastic limit



often cited in the bibliography. The used data to carry out the comparison are obtained from [30] which has been done in the same condition of current work in this research group. Both materials were characterized through a tensile stress, and their stress-strain curves are compared. Factographies taken with a Moticam 3 digital camera through a Motic SMC binocular loupe shall also lead to further detail about the differences between fracture modes. Finally, microscratch tests were conducted in a Scratch tester unit (CSM-Instruments) using a spherical diamond indenter with a radius of 200 μm , to

compare wear resistance of both materials. Tests were done under linearly increasing load, from 0 to 120 N in case of Timberfill and from 0 to 70 N in case of PLA, at a loading rate of 10 mm/min and in an interval length of 5 mm, according to ASTM C1624-05 standard [25]. These tests were conducted along both the longitudinal and transversal printing direction to observe the main plastic deformation mechanisms induced. Surface damage induced during scratch tests was observed by a desktop scanning electron microscopy Phenom XL from ThermoFisher Scientific.

Fig. 5 Main effect for mean effects calculated through ANOVA. Response variable: maximum strength

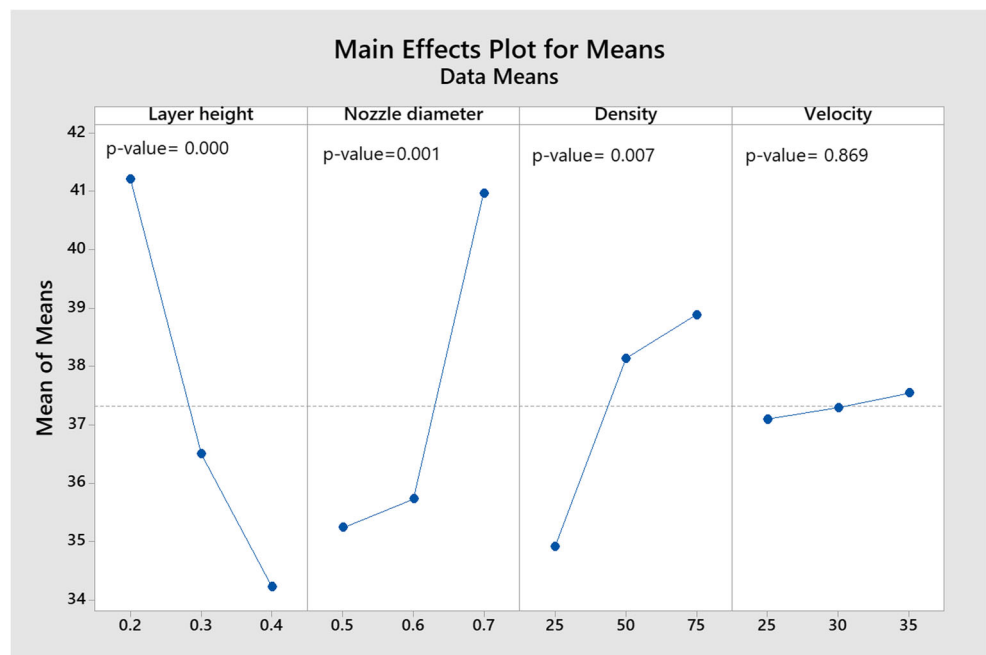


Fig. 6 Main effect for mean effects calculated through ANOVA. Response variable: maximum deformation

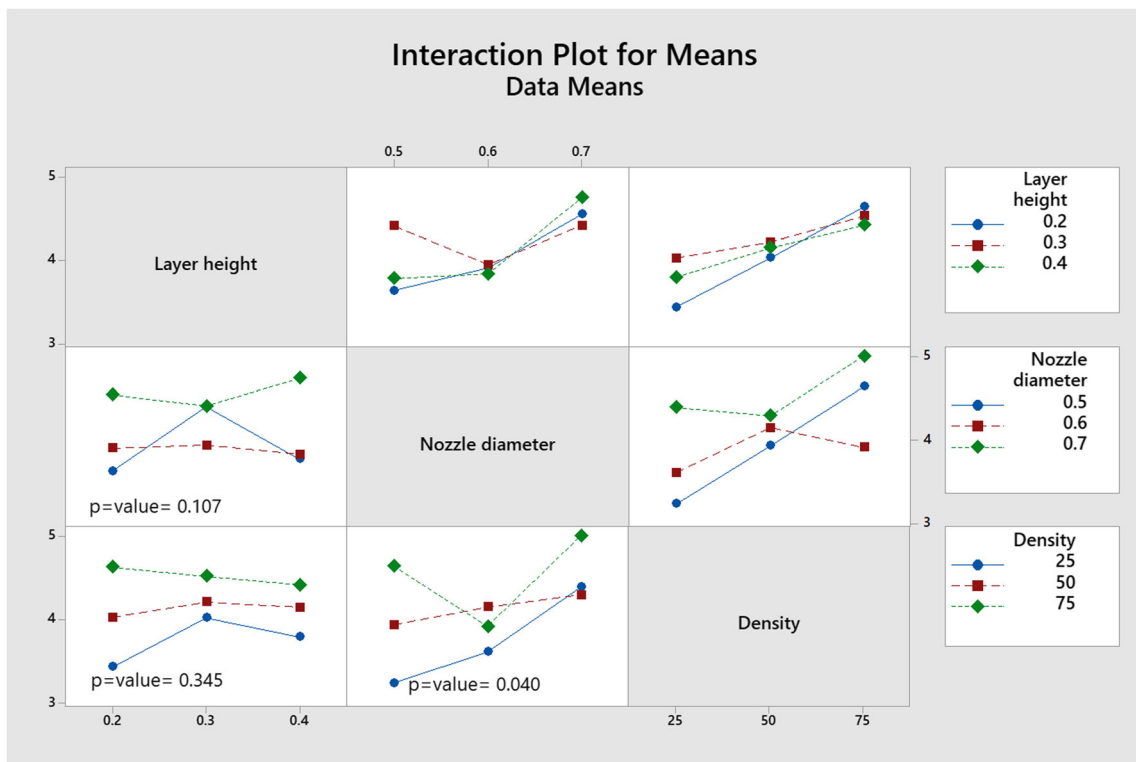
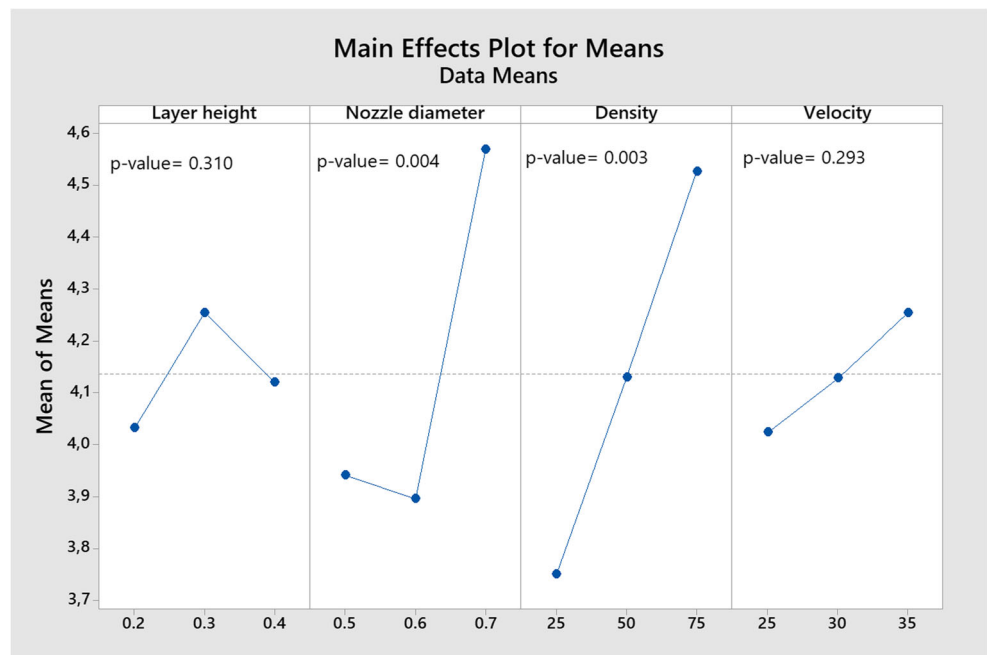


Fig. 7 Main effect for interactions calculated through ANOVA. Response variable: maximum deformation

Table 5 Summary of significances on responses. ↑↑, highly influential parameters. ↑, slightly influential parameters. n.i., non-influential parameters

Factors	Responses			
	Elastic properties		Plastic properties	
	Young’s module (<i>E</i>)	Elastic limit (<i>Rp</i> _{0,2})	Maximum stress (<i>σ</i> _{max})	Maximum deformation (<i>ε</i>)
Layer height (mm)	0.2 ↑↑	0.2 ↑↑	0.2 ↑↑	n.i.
Nozzle diameter (mm)	0.7 ↑↑	0.7↑	0.7 ↑↑	0.7 ↑↑
Fill density (%)	50 ↑	n.i.	75 ↑↑	75 ↑↑
Printing velocity (mm/s)	n.i.	n.i.	n.i.	n.i.

2.7 Comparison between FFF Timberfill and injection-molded Timberfill

Finally, a comparison between the flexural properties of the printed and injected Timberfill was conducted, to evaluate the effects of the additive manufacturing strategy on the material’s properties.

3 Results analysis

The average results of the five repetitions of each manufacturing configuration, including the standard deviation, are included in Table 4.

3.1 Analysis of variance

An analysis of variance (ANOVA) was performed on the dataset included in the Taguchi experimental array, for each parameter that describes the mechanical behavior of the evaluated specimens. To validate the statistical significance of the parameters included in the model on each of the responses, the *p* value associated to the ANOVA was compared to a significance level of 5%.

3.1.1 Young’s module

In this case, it can be concluded that the most significant parameters, due to their *p* values, are the layer height and the

Table 6 Optimized set of parameters and their levels

Factor	Level
Layer height (mm)	0.2
Nozzle diameter (mm)	0.7
Density (%)	75
Printing velocity (mm/s)	35

nozzle diameter as shown in Fig. 3. This graph evidences that the layer height results have an inverse relation with the Young’s module, but higher values of nozzle diameter and density results in a higher elastic module. Based on the obtained *p* values, density can be taken into account because the value is not so much bigger than 0.05, but printing velocity does not show a significant effect on the Young’s module. Increasing the Young’s module by lower height of the layers and bigger diameter of nozzle can be due to the increasing connectivity between the layers by one side, and decreasing the porosity on the other side.

In this case, obtained *p* values were more than 0.05; it means that the selected parameters in this study are independent of each other, at least in the analyzed value ranges for Young’s module.

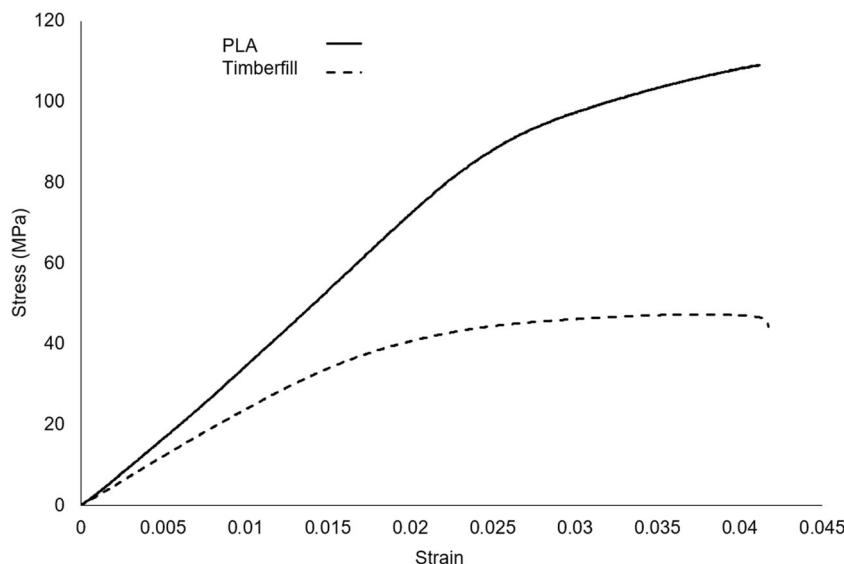
3.1.2 Elastic limit

It is necessary to see how the variation of the different factors affects the elastic limit, which is indicated in the graph of main effects for the averages (Fig. 4). As already mentioned, the most significant parameter due to the *p* value on elastic limit is layer height; that it should be lower to obtain the bigger elastic limit, which in this work is 0.2 mm. On the other side, the nozzle diameter has a direct proportion with the elastic limit; it means the bigger the diameter, the higher elastic limit. This

Table 7 Comparison of factor levels leading to best results for PLA and wood-reinforced PLA

Factor	Material	
	PLA	Timberfill
Layer height (mm)	0.1	0.2
Nozzle diameter (mm)	0.6	0.7
Density (%)	75	75
Printing velocity (mm/s)	20	35

Fig. 8 Strain-stress curve of PLA and wood-reinforced PLA



fact has the same reason to which happened to Young’s module response regarding that both are related to elastic regime. Infill density and printing velocity did not show a significant effect on elastic limit.

Similar to the interaction between parameters on Young’s module, the *p* value does not show significant on limit elastic. It means there is no influential interaction between parameters.

3.1.3 Maximum stress

Based on the obtained *p* values from the factors, it can be mentioned that there is a notable significance of layer height, nozzle diameter, and infill density on the maximum stress. Following, the best levels of these factors are shown in Fig. 5.

In order to the selected variations of the factors in this work, the best level of the layer height, nozzle diameter, and infill density be influent on the maximum stress are 0.2 mm, 0.7 mm, and 75%, respectively. Decreasing the layer height and increasing the nozzle diameter and fill density rises the solidity of the sample to endure the tension more often.

The obtained *p* values of interaction are higher than 0.05, therefore the interaction between parameters should not be taken into account as a significant.

3.1.4 Maximum deformation

In this case, the layer height is not an influential parameter whereas infill density and nozzle diameter have shown significant *p* value on the maximum deformation. In Fig. 6, the best level of these factors could be found.

In order to the selected variations of the factors in this work, the best level of the infill density and nozzle diameter to influence on the maximum deformation are 75% and 0.7 mm, respectively. It is clear that bigger nozzle diameter meant more

voluminous filaments cause more deformation resistance to failure consequently. It can be seen from Fig. 7 that there could be different infarctions between the parameters and levels. As already mentioned, to consider the interaction of parameters influential, the *p* value has to be taken into account. In this case is lower than 0.05 for the interaction between nozzle diameter and density, meaning that the interaction between the levels of both parameters can influence the maximum deformation value.

It is worth mentioning that the signal-to-noise ratio (SN) has been measured to find the robustness of each factor on the selected response variables. Since the most influential parameters were also the most robust ones for each taken response variable and the form of the graphs was totally the same to the graph of the means, it was decided to avoid put all of the graphs.

3.2 Results discussion

An overview of the results is summarized in Table 5. Based on the *p* values, the most influential parameters on the responses are shown with two arrows, whereas those factors that are only slightly influential are associated to one arrow. The best levels for each one are indicated in the cells. Non-influential parameters are also indicated in the table.

Table 8 Comparison of maximum values of all mechanical properties achieved for PLA and wood-reinforced PLA

Material	Timberfill	PLA
Young’s modulus (GPa)	2.41	3.70
Elastic limit (MPa)	38.06	90.80
Maximum stress (MPa)	47.26	109.50
Maximum deformation (%)	5.34	6.21

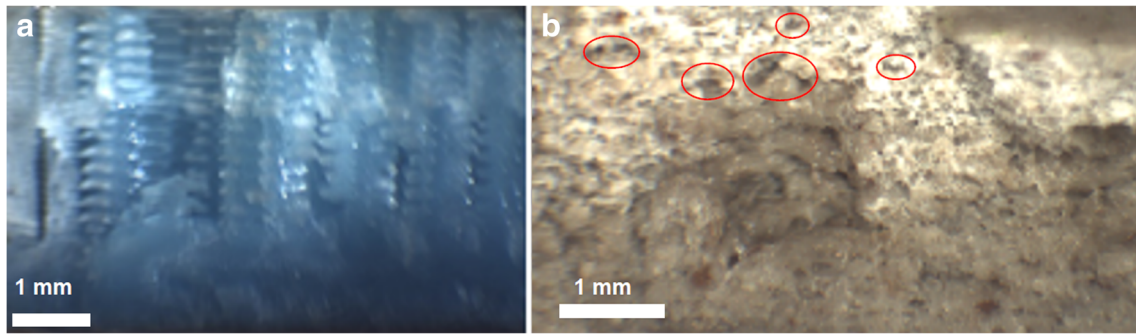


Fig. 9 Fracture section of specimens. **a** PLA specimen with a layer height of 0.1 mm and filament width 0.3 mm. **b** Wood-reinforced PLA specimen

with layer height 0.2 mm and filament width 0.7 mm. Both in 75% infill density

These results evidenced that each of the analyzed parameters is related to a different stress-strain functional regime of the FFF Timberfill material. Whereas the layer height seems to determine how the material endures the stress to which it is subjected during the whole test, the nozzle diameter and the fill percentage are clearly more influential in how the Timberfill works in its plastic regime, as well as its failure mode as proves the maximum deformation registered in the tests. For this reason, a single optimal parameter set cannot be defined. Since the height of the layers should not exceed half of the nozzle diameter, the lower height of layers resulted as the bigger nozzle diameter. These phenomena could be because of the enough adhesion between the layers and make the samples more stiff consequently. Increasing the solidity percentage of inside the samples based on the infill density results to more endurance and the samples resist more to failure as well.

In this situation, the criteria that will be followed in order to define the best level for each parameter are based on the following two conditions:

- If a parameter delivers the best response at the same level in all cases, it is chosen.
- In case of divergence, then the level with the lowest *p* value in the ANOVA test is chosen.

Table 6 shows the final result for the optimized set of parameters. It is worth mentioning that, as the printing velocity is not influential in any case, the highest value has been taken for the sake of productivity.

3.3 Comparison between Timberfill and PLA

Table 7 shows the best combination set of parameters obtained for PLA and Timberfill material. The results related to PLA specimens have been extracted from previous research published by the authors in [30].

The direct comparison of both materials proves that they demand a low value of layer height combined with a higher nozzle diameter, and a 75% infill density, so that their mechanical properties are enhanced. Indeed, by decreasing the height

Fig. 10 Microscratch tests. **a** Wood-reinforced PLA. **b** PLA

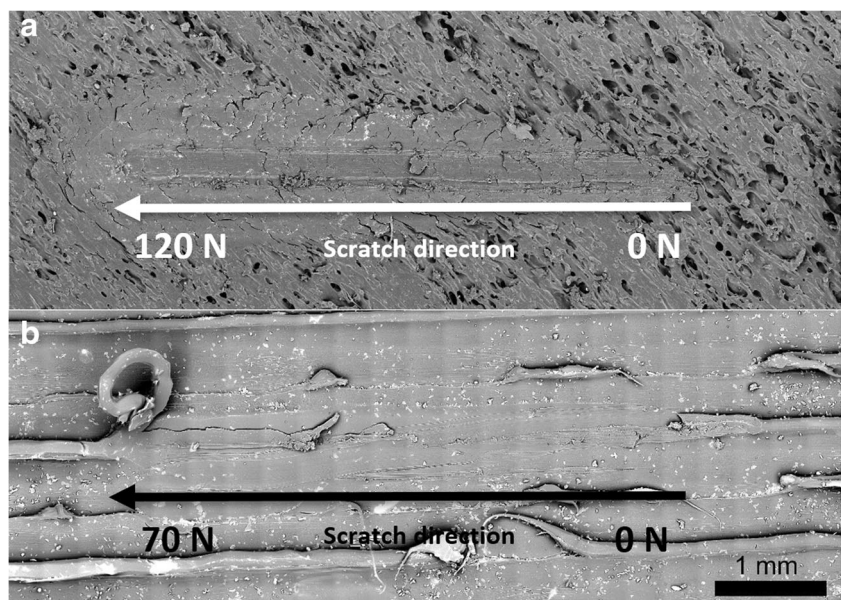
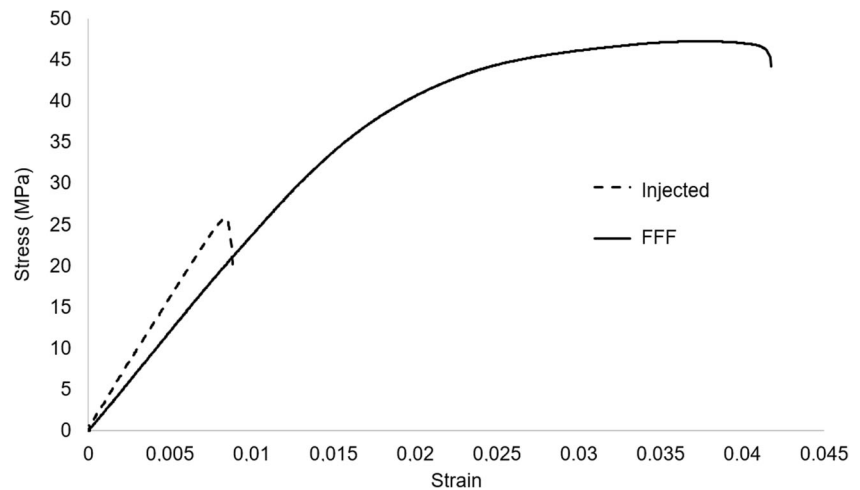


Fig. 11 Strain-stress curve of FFF and injected wood-reinforced PLA



between layers and increasing the material flow, as well as depositing each filament with the lowest offset to the adjacent one, leads to a net increase of the enduring material, thus enhancing the overall resistance of the material. On the other hand, printing velocity results are reversed, although it must be highlighted that 20 mm/min resulted in better results for the PLA, and was non-influential in the Timberfill material. The presence of wood could be the cause to this divergence.

Although the direct comparison of the optimal levels has proved a similar influence of both materials, it is also necessary to compare the absolute results represented by two respective illustrative strain-stress curves (Fig. 8). The absolute values are shown in Table 8. The introduction of wood in the PLA matrix is clearly detrimental to the mechanical behavior of the Timberfill.

The examination of a fractography can lead to further information about this phenomenon. Indeed, the wood fibers create discontinuities in the matrix causing lower ductility in Timberfill with respect to PLA. That is also corroborated by the microscopy pictures of fracture cross-section taken by the same camera (Fig. 9). Some examples of segregated wood particles looking like porosity defects are highlighted in Fig. 9b.

As a first approach, the presence of wood inside the PLA matrix could lead to think that it increases the inner friction of the material, thus increasing its resistance and restricting its deformation. However, the wood fibers are actually acting as an anchor that transfers the load to the PLA matrix and its fibers. Therefore, the crack is forced to advance through these particles, which are perpendicular to the stress, with a consequent stress concentration, and an overall decrease of the mechanical resistance to bend the Timberfill material.

To better understand the fracture behavior, micro scratch tests were performed on both materials (Fig. 10). It is confirmed that Timberfill is formed as a porous material, as discussed above. The base PLA deformed by the scratch partially covers the remaining pores of the sample. Up to the

tested force in both materials (120 N for Timberfill, 70 N for PLA), they both show a ductile behavior, without evidencing cracking in the base material. Neither of them shows remarkable adhesive wear. On the other hand, there are no disclosures between filaments in any of the materials, fact that implies that the adhesion between filaments in the same layer is enough to resist the efforts applied during the test.

What is clearly different between the two materials is the obtained friction coefficient, being 0.4 for Timberfill, twice than for the PLA. In both cases, the value is kept constant throughout the test. At sight of the obtained results in the scratch tests, it can be stated that the introduction of the wood inside the PLA matrix to create the Timberfill composite increases the friction of the material, that could be interesting for certain future applications of the material.

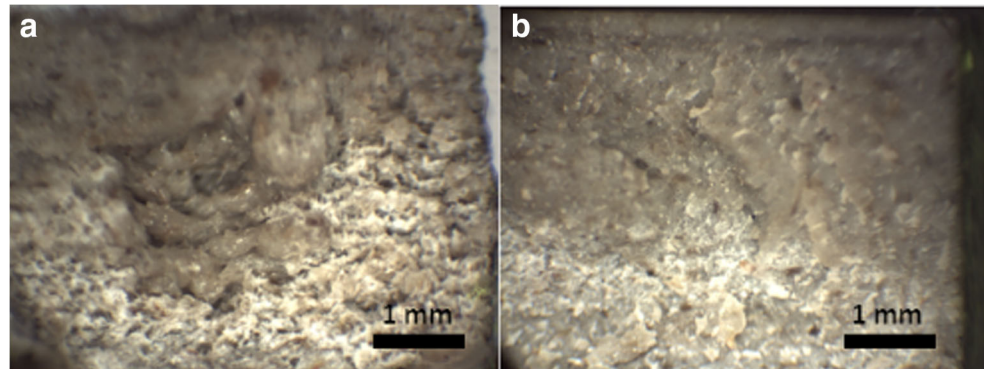
3.4 Comparison between FFF Timberfill and injected Timberfill

Bending engineering stress-strain curves for printed and injected samples are shown in Fig. 11. The Young's modulus of the additive manufactured samples was 2.41 GPa, almost 75% of the injected samples (3.11 GPa), but the other properties were higher in the FFF specimens than on the completely solid ones. For example, the average values of flexural

Table 9 Comparison of maximum values of all mechanical properties achieved for injected and FFF wood-reinforced PLA

Maximum values		
Timberfill	Printed	Injected
Young's modulus (GPa)	2.41	3.11
Elastic limit (MPa)	38.06	24.62
Maximum stress (MPa)	47.26	25.62
Maximum deformation (%)	5.34	1.02

Fig. 12 Fracture zone of wood-reinforced PLA parts. **a** FFF. **b** Injected



strength were 38.06 and 24.62 MPa for printed and injected samples, respectively (Table 9), meaning that the processing of the Timberfill material by FFF enhances the overall behavior of the material.

To specify this observation, microscopic examinations of the specimens' cross-section were performed. Figure 12 a shows the specimen with honeycomb pattern at a 75% infill density, and Fig. 12 b shows the injected sample. The brightened zones represent the area subjected to tensile effect. Regarding to the obtained values for responses (Table 9) and the behavior shown in the fracture, it is noticeable that the specimen generated by successive filaments shows a higher ductility due to the fact that these filaments have higher mobility one with respect to the other. Thus, the crack growth property which occurs in the outer fiber of the sample can decrease the ductility of injected parts, because this phenomenon should repeat for each layer of printed parts. Likewise, lower height of the layers and bigger diameter of the nozzle help adhesion between consecutive layers. This can consequently increase the maximum stress and flexural resistance of the printed samples.

Finally, the printed specimens demonstrated more resistance than injected samples when they are submitted to bending forces. This means that the FFF process must be recommended over the classical injection method to manufacture wood-composite PLA pieces, which are expected to be loaded according to bending moments.

4 Conclusions

The experiments conducted through the research explained in this paper have enriched the knowledge about an innovative wood-reinforced PLA material used for additive manufacturing systems. Firstly, it was found that by combining a 0.2-mm layer height, 0.7-mm nozzle diameter, and 75% infill density, the material exhibits the best mechanical properties, regardless of the printing velocity set to the system. Of all those parameters, the layer height proves to be the most influential one, followed by the nozzle diameter, whereas no interaction

between them seems to be important to determine the mechanical behavior of the obtained specimens. This result evidences that a lower height of the layers combined with a higher nozzle diameter delivers a stronger adhesion between the layers that enhances the resistance of the additive manufactured parts.

On the other hand, valuable information about the composite material has been found when comparing it to non-reinforced PLA, as wood particles have proved to hinder the mechanical resistance of the material due to the fact that they increase the void between filaments and prevent neck growth between them. For this reason, the introduction of wood as a mechanical enhancer should be unadvised, and the wood-reinforced PLA should only be used in applications where mechanical properties are not relevant. An unexplored aspect of the matter in this paper is whether changing the actual composition of wood fiber inside the PLA matrix could be effective in turn positively effective on the resistance properties of the composite material.

Finally, the comparison of FFF specimens to injected ones has also proved that the mechanical properties of wood-reinforced PLA or Timberfill material should be processed through additive manufacturing to maximize its properties. The maximum deformation experienced by FFF specimens was fivefold than those obtained through injection, that could be caused by the interaction between filaments and solidity percentage of the workpieces that increase the ductility of the workpiece.

Funding information J.J. Roa acknowledges the Serra Hünter programme of the Generalitat de Catalunya for the financial support.

Data availability The raw/processed data required to reproduce these findings cannot be shared at this time as the data also forms part of an ongoing study.

References

1. Chia HN, Wu BM (2015) Recent advances in 3D printing of biomaterials. *J Biol Eng* 9(1):4
2. Brenken B, Barocio E, Favaloro A, Kunc V, Pipes RB (2018) Fused filament fabrication of fiber-reinforced polymers. A review. *Addit Manuf* 21:1–16

3. Cuan-Urquiza E, Barocio E, Tejada-Ortigoza V, Pipes RB, Rodriguez CA, Roman-Flores A (2019) Characterization of the mechanical properties of FFF structures and materials. A review on the experimental, computational and theoretical approaches. *Materials (Basel)* **12**(6)
4. Jerez-Mesa R, Travieso-Rodríguez JA, Llumà-Fuentes J, Gomez-Gras G, Puig D (2017) Fatigue lifespan study of PLA parts obtained by additive manufacturing. *Procedia Manuf* **13**:872–879
5. Afrose MF, Masood SH, Lovenitt P, Nikzad M, Sbarski I (2015) Effects of part build orientations on fatigue behaviour of FDM-processed PLA material. *Progress Addit Manuf* **1**(1–2):21–28
6. Gomez-Gras G, Jerez-Mesa R, Travieso-Rodríguez JA, Llumà-Fuentes J (2018) Fatigue performance of fused filament fabrication PLA specimens. *Mater Des* **140**:278–285
7. Es-Said OS, Foyos J, Noorani R, Mendelson M, Marloth R, Pregger BA (2000) Effect of layer orientation on mechanical properties of rapid prototyped samples. *Mater Manuf Process* **15**:107–122
8. Wu W, Geng P, Li G, Zhao D, Zhang H, Zhao J (2015) Influence of layer thickness and raster angle on the mechanical properties of 3D-printed PEEK and a comparative mechanical study between PEEK and ABS. *Materials (Basel)* **8**(9):5834–5846
9. Shabat D, Rosenthal Y, Ashkenazi D, Stern A (2017) Mechanical and structural characteristics of fused deposition modeling ABS material. *Annals of “Dunarea de Jos” University, Fascicle XII, Welding Equipment and Technology* **28**:16–24
10. Sood AK, Ohdar RK, Mahapatra SS (2010) Parametric appraisal of mechanical property of fused deposition modelling processed parts. *Mater Des* **31**:287–295
11. Araya-Calvo M, López-Gómez I, Chamberlain-Simon N, León-Salazar JL, Guillén-Girón T, Corrales-Cordero JS (2018) Evaluation of compressive and flexural properties of continuous fiber fabrication additive manufacturing technology. *Addit Manuf* **22**:157–164
12. El Margi A, El Mabrouk K, Vaudreui S, Ebn Touhami M (2019) Mechanical properties of CF-reinforced PLA parts manufactured by fused deposition modeling. *J Thermoplast Compos Mater* p. 0892705719847244
13. Jo MY, Ryu YJ, Ko JH, Yoon JS (2012) Effects of compatibilizers on the mechanical properties of ABS/PLA composites. *J Appl Polym Sci* **125**(S2):E231–E238
14. Rosenzweig DH, Carelli E, Steffen T, Jarzem P, Haglund L (2015) 3D-printed ABS and PLA scaffolds for cartilage and nucleus pulposus tissue regeneration. *Int J Mol Sci* **16**(7):15118–15135
15. Cantrell JT, Rohde S, Damiani D, Gurmani R, DiSandro L, Anton J, Young A, Jerez A, Steinbach D, Kroese C, Ifju PG (2017) Experimental characterization of the mechanical properties of 3D-printed ABS and polycarbonate parts. *Rapid Prototyp J* **23**(4):811–824
16. Tymrak BM, Kreiger M, Pearce JM (2014) Mechanical properties of components fabricated with open-source 3-D printers under realistic environmental conditions. *Mater Des* **58**:242–246
17. Bagheri A, Buj-Corral I, Ferrer M, Pastor MM, Roure F (2018) Determination of the elasticity modulus of 3D-printed octet-truss structures for use in porous prosthesis implants. *Materials* **11**(12):2420
18. Ozcelik B, Ozbay A, Demirbas E (2010) Influence of injection parameters and mold materials on mechanical properties of ABS in plastic injection molding. *Int Commun Heat Mass Transfer* **37**(9):1359–1365
19. Casavola C, Cazzato A, Moramarco V, Pappalettere C (2016) Orthotropic mechanical properties of fused deposition modelling parts described by classical laminate theory. *Mater Des* **90**:453–458
20. Quintana R, Choi JW, Puebla K, Wicker R (2009) Effects of build orientation on tensile strength for stereolithography-manufactured ASTM D-638 type I specimens. *Int J Adv Manuf Technol* **46**(1–4):201–215
21. Galantucci LM, Lavecchia F, Percoco G (2010) Quantitative analysis of a chemical treatment to reduce roughness of parts fabricated using fused deposition modeling. *CIRP Ann* **59**:247–250
22. Maidin S, Mohamed AS, Akmal S, Mohamed SB, Wong JHU (2018) Feasibility study of vacuum technology integrated fused deposition modeling to reduce staircase effect. *Journal of Fundamental and Applied Sciences* **10**(1S):633–645
23. Lederle F, Meyer F, Brunotte GP, Kaldun C, Hübner EG (2016) Improved mechanical properties of 3D-printed parts by fused deposition modeling processed under the exclusion of oxygen. *Progress Addit Manuf* **1**(1-2):3–7
24. Malinauskas M, Reškšytė S, Lukoševičius L, Butkus S, Balčiūnas E, Pečiukaiytė M, Baltriukienė B, Bukelskienė V, Butkevičius A, Kucevičius P, Rutkūnas V, Juodkzasis S (2014) 3D microporous scaffolds manufactured via combination of fused filament fabrication and direct laser writing ablation. *Micromachines* **5**(4):839–858
25. Abedini A, Asiyabi T, Campbell HR, Hasanzadeh R, Azdast T (2019) On fabrication and characteristics of injection molded ABS/Al₂O₃ nanocomposites. *Int J Adv Manuf Technol* **102**(5–8):1747–1758
26. Nejad SJ, Hasanzadeh R, Doniavi A, Modanloo V (2017) Finite element simulation analysis of laminated sheets in deep drawing process using response surface method. *Int J Adv Manuf Technol* **93**(9–12):3245–3259
27. De Ciurana J, Serenóa L, Vallès È (2013) Selecting process parameters in RepRap additive manufacturing system for PLA scaffolds manufacture. *Procedia CIRP* **5**:152–157
28. Testing A.S.f. and Materials. Standard test method for flexural properties of unreinforced and reinforced plastics and electrical insulating materials by four-point bending. (2002) ASTM International
29. Mohamed OA, Masood SH, Bhowmik JL (2015) Optimization of fused deposition modeling process parameters a review of current research and future prospects. *Adv Manuf* **3**:42–53
30. Travieso-Rodríguez JA, Jerez-Mesa R, Llumà J, Traver-Ramos O, Gomez-Gras G, Roa Rovira JJ (2019) Mechanical properties of 3D-printing polylactic acid parts subjected to bending stress and fatigue testing. *Materials* **12**(23):3859

Publisher's note Springer Nature remains neutral with regard to jurisdictional claims in published maps and institutional affiliations.